photonics

MDPI

Communication

Ultrashort Pulses of 32 W and 207 fs at 1 MHz from a Compact All-Fiber Amplifier

Xin Shao [1], Xianghao Meng [1,*], Tianmeng Jiao [1], Zhaoqing Gong [1], Jie Yang [1], Xianglong Zhao [1], Guangdao Yang [1], Yang Bi [1], Jiahui Chen [1] and Pingxue Li [1,2]

[1] Faculty of Physics and Optoelectronic Engineering, Beijing University of Technology, Beijing 100124, China; shaoxin@emails.bjut.edu.cn (X.S.); jtmly@emails.bjut.edu.cn (T.J.); gongzhaoq@emails.bjut.edu.cn (Z.G.); yj.bjut.edu.cn@emails.bjut.edu.cn (J.Y.); zxlong@emails.bjut.edu.cn (X.Z.); gdyang3105@emails.bjut.edu.cn (G.Y.); biyang@emails.bjut.edu.cn (Y.B.); chenjiahui314@emails.bjut.edu.cn (J.C.); pxli@bjut.edu.cn (P.L.)

[2] Key Laboratory of Materials Low-Carbon Recycling, Beijing University of Technology, Beijing 100124, China

* Correspondence: xhmeng@bjut.edu.cn

Abstract

We have demonstrated a high-power, polarization-maintaining all-fiber amplifier operating at a repetition rate of 1 MHz. The seed laser is a Semiconductor Saturable Absorber Mirror (SESAM) mode-locked oscillator with an 18.1 nm full width in half-maximum (FWHM) spectrum. The pulse duration is stretched to 1.1 ns using temperature-controlled chirped fiber Bragg gratings (TCFBGs) and subsequently amplified in a 40 μm core Yb-doped fiber, achieving a maximum output power of 37 W. The amplified laser exhibits excellent beam quality with an M^2 factor of 1.04. The pulse duration is compressed to 207 fs in a single-grating compressor with 86% efficiency, yielding an average power of 32 W, a pulse energy of 32 μJ, and a peak power of 154.6 MW. This high-power all-fiber femtosecond laser is a promising source for scientific and industrial applications.

Keywords: chirped pulse amplification; femtosecond laser; fiber laser

1. Introduction

Ultrafast fiber lasers offer unique advantages, including high average power, excellent beam quality, reliability, compactness, and maintenance-free operation, making them advanced laser sources for diverse application fields. These encompass biomedical imaging, optical communications, harmonic generation, optical frequency combs, and the optical dynamics of soliton lasers [1–4]. Particularly in ultrafast laser micromachining, various processes have been investigated, including ablation, drilling, glass welding, and scribing [5–8]. Due to the structural characteristics of optical fibers, pulses are confined to propagate within the micrometer-scale core. The resulting strong nonlinear effects degrade the pulse quality output from fiber amplifiers. To mitigate the impact of nonlinear effects, two primary approaches have been extensively developed: temporally stretching pulses using Chirped Pulse Amplification (CPA) techniques and spatially increasing the mode field area through Large Mode Area (LMA) fiber designs.

Photonic Crystal Fibers (PCFs), which combine large mode field areas with polarization-maintaining (PM) single-mode transmission, represent a crucial pathway for further enhancing laser beam quality and meeting the performance demands of high-power lasers. The main amplification stage employs a rod-type PCF as the gain medium, effectively suppressing higher-order modes and reducing nonlinear accumulation [9–14]. This enables

Check for updates

Received: 19 January 2026
Revised: 30 January 2026
Accepted: 16 February 2026
Published: 28 February 2026

Copyright: © 2026 by the authors. Licensee MDPI, Basel, Switzerland. This article is an open access article distributed under the terms and conditions of the Creative Commons Attribution (CC BY) license.

high-power or high-single-pulse-energy laser output. Although rod-type PCF as the gain medium in the CPA system enables an output power of 248 W [15], spatial coupling is required for these fibers. This requirement hinders the realization of an all-fiber structure and compromises the compactness and environmental stability of the fiber laser. For all-fiber CPA systems, relatively small-core double-clad LMA fibers can also be directly spliced to achieve high-power laser output. In 2016, the output characteristics of an all-fiber CPA laser were optimized by balancing nonlinear effects with output power to suppress Raman shift in the main amplifier. At a repetition rate of 200 kHz, an average power output of 10 W was obtained, with pulses compressed to 933 fs [16]. That same year, an all-fiber CPA laser based on Yb-doped Fibers (YDFs) with a core/cladding diameter of 30/250 μm yielded an output with a repetition rate of 17.57 MHz, a single pulse energy of 7.22 μJ, and a compressed pulse duration of 566 fs [17]. In 2019, at a low repetition rate of 1 kHz, a synchronously pumped technique effectively suppressed ASE during amplification. Using a 30/250 μm fiber, an output of 180 fs pulses with 112 mW power at 1030 nm was achieved [18]. In 2023, by employing parabolic shaping to effectively mitigate subsequent nonlinear effects, laser output with a pulse duration of 143 fs, an average power of 8.57 W, and a single-pulse energy of 85.7 μJ was ultimately achieved [19]. In 2024, a highly stable, ultrafast ultraviolet source based on a PM all-fiber laser is reported. Operating at a repetition rate of 28.9 MHz, it delivers a maximum output power of 9.39 W with a compressed pulse duration of 244 fs [20]. In 2025, a repetition-rate tunable Yb-doped fiber laser system is demonstrated. It generates pulses with energy of 1 μJ and duration of 143 fs at 2 MHz, and pulses with energy of 10 μJ and duration of 157 fs at 200 kHz [21]. However, longer gain fibers are typically required to provide sufficient gain, leading to severe nonlinear effects and accumulation of higher-order dispersion, as well as poor beam quality.

Recently, flexible PCF has been employed as the gain fiber in CPA systems as the main amplifier. In 2018, an experimental study on fully welded PCF femtosecond CPA was reported, achieving a compressed average power of up to 9.8 W at a repetition rate of 275 kHz with a pulse duration of 495 fs [22]. In 2019, amplification was achieved in a PCF with a core/cladding diameter of 40/200 μm, achieving an output power of 17.5 W with a pulse duration of 172 fs [23]. In 2021, a nonlinear CPA technique was reported, utilizing self-phase modulation in a fiber stretcher for pulse shaping. At a repetition rate of 1 MHz, it delivered a duration of 382 fs and an average power of 20 W [24]. This method combines the advantages of LMA fibers and rod-type PCFs, it ensures beam quality and enhances the nonlinear effect threshold without requiring complex spatial coupling. Precise control of the PCF length effectively reduces the accumulation of higher-order dispersion, making it an approach for generating high-power femtosecond fiber lasers. Figure 1 shows the performance comparison of all-fiber amplifiers in terms of pulse duration and average power.

In this letter, we report an integrated CPA system employing an all-fiber amplifier. Flexible fusion splicing technology for LMA-PCF overcomes the limitations of free-space coupling in the amplification chain of conventional fiber lasers. The system delivers up to 32 W of compressed average power (32 μJ pulse energy) at a 1 MHz repetition rate, with pulses compressed to 207 fs using a free-space grating pair.

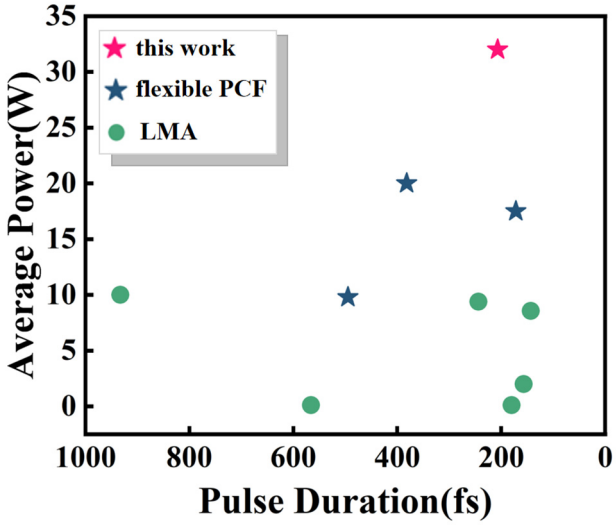


Figure 1. Performance of all-fiber amplifiers in terms of pulse duration and average power.

2. Experimental Setup

The experimental schematic of the high-power femtosecond fiber laser is shown in Figure 2. It consists of four main sections: a custom-built SESAM mode-locked broadband fiber oscillator, a fiber stretcher, multiple amplifier stages, and a grating compressor. The main amplifier stage utilized a gain fiber with a core diameter of 40 μm and a cladding diameter of 140 μm. The system oscillator consists of SESAM and a chirped fiber Bragg grating (CFBG, TeraXion Inc., Quebec, Canada), which also serves as a dispersion management element. The CFBG had a reflectivity of 15% and provided anomalous dispersion with $\beta_2 = -0.20$ ps^2. Its reflection spectrum featured a Gaussian profile centered at 1030 nm with a 3 dB bandwidth of 20 nm. Gain was provided by a 1 m long YDF (Nufern, East Granby, USA, PM-YSF-HI-HP, absorption of 250 dB/m at 976 nm) pumped by a single-mode laser diode (LD). Pulses were extracted from the 20% port of the output coupler.

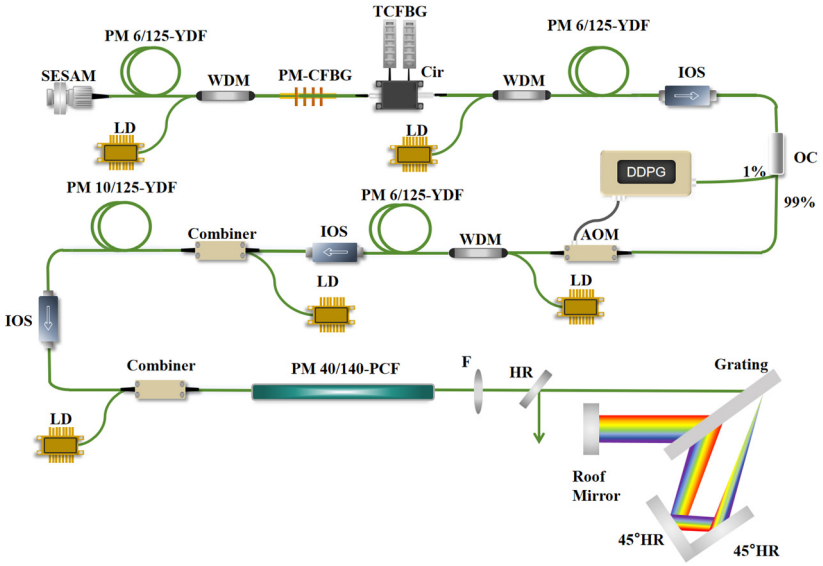


Figure 2. Experimental setup of the high-power CPA system. WDM: wavelength division multiplexer; ISO: isolator; Cir: circulator; CFBG: chirped fiber Bragg grating; PM-YDF: polarization-maintaining ytterbium-doped fiber; OC: optical coupler; Combiner: pump/signal combiner; F: Focusing lens; HR: High-reflection mirror.

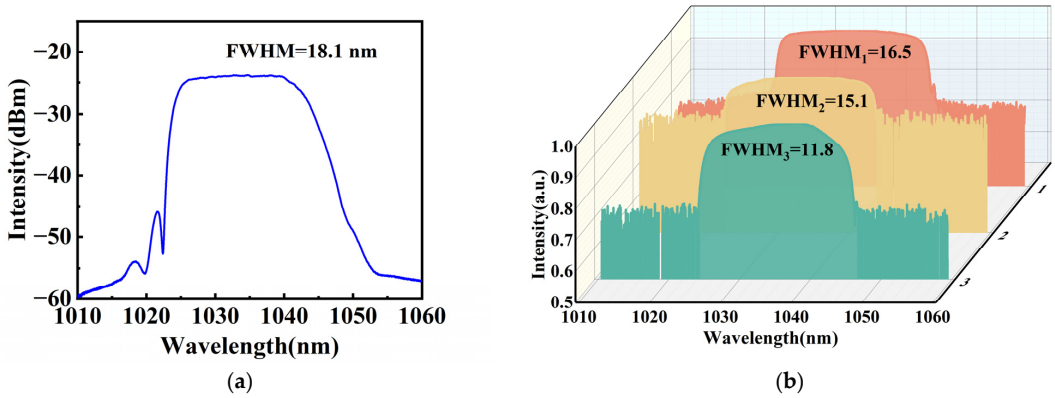
The oscillator output laser was first directed into a pulse stretcher comprising two TCFBGs (Teraxion, TPSR). The TCFBGs were connected via a four-port circulator, providing a group velocity dispersion (GVD) of -55.54 ps/nm and a tunable range of ± 0.45 ps^2, and a third-order dispersion (TOD) of -0.0205 ps/nm^2 with a tunable range of ± 0.01 ps^3. The reflection spectrum was centered at 1035 nm with a 3 dB bandwidth of 20 ± 2 nm. Subsequently, the stretched pulse underwent power amplification in the first pre-amplifier stage. This stage employed a 1 m long YDF with a core/cladding diameter of 6/125 μm, core-pumped via a wavelength division multiplexer (WDM) by a 976 nm single-mode LD. Following an isolator, an optical coupler (OC) splits the laser into 1% and 99% branches. A second pre-amplifier stage, also using a 1 m long YDF with 6/125 μm core/cladding diameter, compensated for the power loss induced by the acousto-optic modulator (AOM). The third pre-amplifier stage utilized cladding pumping, with a 1.4 m long double-clad YDF (Nufern, PLMA-YSF-10/125, absorption of 4.9 dB/m at 976 nm) with a core/cladding diameter of 10/125 μm as the gain medium. The main amplifier incorporated a 0.35 m long LMA-PCF (PLMA-YDF-40/140 μm, absorption of 22 dB/m at 976 nm), made by the Shanghai Institute of Optics and Fine Mechanics, Chinese Academy of Sciences, China. This fiber features a mode field diameter of 30 μm and a core diameter of 40 μm. The gain fiber is directly fusion-spliced to the pump beam combiner to eliminate spatial coupling. Splicing loss is 0.5 dB, a high loss due to lack of mode field matching. For thermal management, the entire PCF is housed in a metal shell with water-cooling channels. This ensures that the splice point and the entire fiber maintain stable temperatures, preventing excessive heat buildup. The final compression stage employs a lens for laser beam collimation. To ensure high stability and integration, the compressor consisted of a single-grating transmission grating with 1700 lines/mm and two 45° mirrors, providing the required optical path within a compact, limited space. The transmission grating measured $136 \times 26 \times 6$ mm^3.

3. Results and Discussions

The output characteristics of the seed laser determine the ultimate performance of high-power ultrashort-pulse fiber laser systems. An ideal seed laser requires a broad spectral bandwidth, a smooth spectral profile, and linear chirping. Through dispersion compensation techniques, the cavity length was strictly controlled. The constructed oscillation cavity measures 2.38 m in length. Figure 3a displays the mode-locked spectral output, with a FWHM of 18.1 nm. This custom near-zero dispersion passive mode-locked laser achieves 2 mW average output power at 50 mW pump power. The repetition frequency is 43 MHz, with a signal-to-noise ratio of 75 dB. We also measured the pulse duration directly from the oscillator. A chirped pulse of 2.2 ps was measured. This broadband fiber-locked laser demonstrates significant potential for generating ultrafast femtosecond pulses.

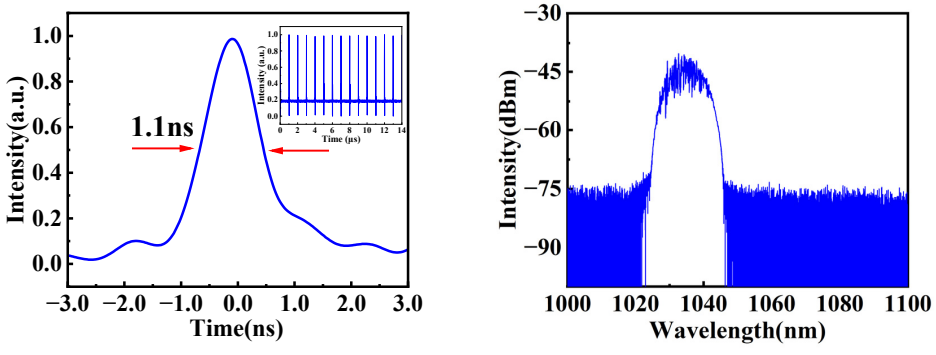
Traditional lasers utilize hundreds of meters of single-mode fiber to achieve second-order dispersion, which is necessary for pulse broadening [25,26]. Normal dispersion fibers function as pulse spreaders, while bulk grating pairs serve as pulse compressors. This technique benefited from the compactness and stability of the fiber stretcher but faced issues with the TOD mismatch between the fiber stretcher and grating compressor, both of which exhibit positive TOD. The accumulation of positive dispersion shift results in a broadened pulse base during compression, leading to dispersed energy and peak power reduction. To precisely control dispersion during amplification, suppress nonlinear effects, and maintain spectral integrity, this study employs a thermally controlled stretcher. Selecting a CFBG with a larger reflection bandwidth can prevent narrowing of the seed spectrum. Thus, a TCFBG with a center wavelength of 1035 nm and a reflection bandwidth of 20 nm was chosen. This pulse stretcher does not filter the seed spectrum during temporal, ensuring minimal impact on the signal spectrum. This computer-controlled device en-

ables precise adjustment to achieve group delay dispersion (GDD) and TOD. As shown in Figure 4a, the broadened seed pulse width measured by an optical detector and oscilloscope is 1.1 ns. Due to insertion losses in the CFBG and circulator, the output power decreases to 1.53 mW. During first-stage preamplification using a core-pumped 6/125 μm Yb-doped single-mode gain fiber, the output power increased linearly with pump power. The stretched signal power amplified from 1.53 mW to 146 mW. Due to the gain narrowing caused by amplification, the $FWHM_1$ of the spectrum decreased to 16.5 nm. The pulse output from the preamplifier subsequently passes through an OC. Its 1% branch provides a trigger signal to the DDPG module driving the AOM, enabling repetition rate modulation and achieving a 43-fold frequency division. Meanwhile, the 99% branch reduces the repetition rate to 1 MHz via the AOM, with the output power decreasing to 2 mW after downconversion. The inset in Figure 4a illustrates the down-converted pulse train. This pulse extraction process introduces significant power loss. The final pulse train is amplified to 69.2 mW by a second-stage 6/125 μm Yb-doped single-mode gain fiber (core-pumped) before entering the final preamplifier. The second-stage preamplifier output spectrum has a $FWHM_2$ of 15.1 nm. The third-stage preamplification employs a 10/125 μm gain fiber, ensuring single-mode operation near 1030 nm to maintain beam quality and prevent multimode degradation [27]. After three-stage preamplification, the average output power reaches 2 W. The final preamplifier stage employs fiber with lower dopant concentration, resulting in significant spectral gain narrowing and a $FWHM_3$ reduction to 11.8 nm. The output spectrum of the three-stage preamplifier is shown in Figure 3b. During the preamplification stage, a 6/125 μm to 10/125 μm gain fiber transition is employed. By increasing the mode field area to reduce power density, the cumulative effects of nonlinear phase shift are effectively suppressed. The gain narrowing effect generated during amplification also suppresses spectral broadening caused by self-phase modulation (SPM).



(**a**) (**b**)

Figure 3. (**a**) Seed laser output spectrum. (**b**) Pre-amplified output spectrum. The red, yellow, and green lines represent the first, second, and third stages of pre-amplification, respectively.



(**a**) (**b**)

Figure 4. *Cont.*

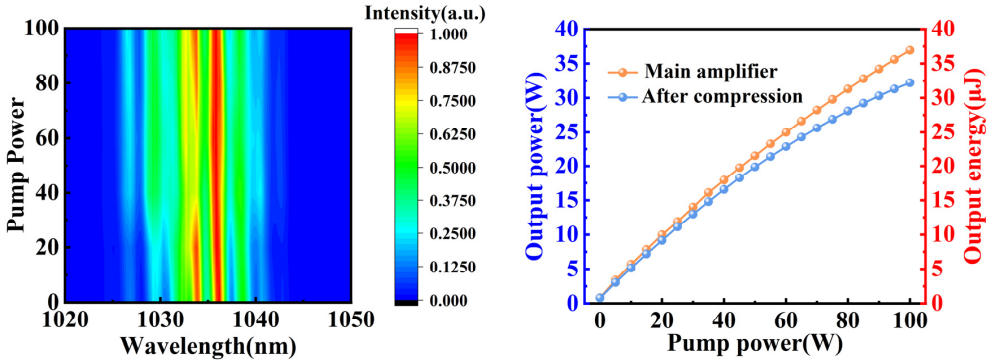


Figure 4. (**a**) Autocorrelation trace of stretched pulses (red arrow: FWHM); Inset: Picked pulse train waveform at a rep-rate of 1 MHz; (**b**) Output spectrum of main amplifier; (**c**) Output spectrum of the main amplifier at different pump power; (**d**) Yellow line: Output power and energy from the main amplifier; Blue line: Power and energy output after compressor.

The nonlinearities experienced by the laser pulse during amplification directly affect the spectral and temporal performances. Even moderately intense SPMs can severely distort and recompress the pulse after amplification, leading to reduced peak power and temporal contrast. Therefore, these effects must be rigorously suppressed [28]. LMA fiber effectively mitigates nonlinear effects during amplification. Its enlarged mode field area permits larger incident spot sizes, significantly reducing power density and preventing permanent fiber damage caused by energy accumulation. To suppress unwanted nonlinear effects and dispersion accumulation in the gain fibers, the fiber length in the main amplifier should be minimized. The B-integral is commonly used to characterize the cumulative effect of nonlinear phase shift in fiber-optic pulses.

$$B = \gamma P_0 \left\{ \frac{exp(gL_g) - 1}{g} + exp(gL_g)L_p \right\} \quad (1)$$

where γ represents the nonlinear parameter, P_0 represents the peak power of the input signal, g represents the gain coefficient of the fiber, and L_g and L_p represent the length of the gain and the passive fiber, respectively. An effective method to reduce the main amplifier B-integral is to shorten the corresponding lengths of the active and passive fibers. With L_p = 0.2 m and L_g = 0.35 m, the pump light absorption efficiency reaches 83%. The B-integral of the main amplifier is 1.14 π rad at an operating power of 37 W. At a pump power of 100 W, the system can deliver an average output power of 37 W. The output spectrum of the main amplifier (Figure 4b) displayed a 3 dB bandwidth of 9.5 nm. The spectrum in Figure 4b confirms that the effects of SRS and ASE are negligible. The generation of the multi-peak spectrum primarily stems from the intense interaction between SPM and the normal dispersion of the optical fiber during high-power pulse propagation. The peak power of the output pulse from the main amplifier exceeds 50 kW. When such high-intensity pulses propagate through a PCF with normal dispersion, the strong phase modulation induced by SPM significantly broadens the spectrum. Figure 4c shows the output spectrum of the main amplifier at different pump power, as the pump power increases, spectral broadening induced by SPM is observed. In the normal dispersion regime, this broadening evolves into spectral sidebands with distinct oscillatory structures, which visually appear as multiple peaks [29]. Increasing pulse energy further would exacerbate SPM, degrading pulse compressibility. After compression, the power reached 32 W, corresponding to a compression efficiency of 86% and a pulse energy of 32 μJ (Figure 4d). The grating is coated with a high-damage-resistant dielectric film. The compression loss arises primarily from

the grating's diffraction efficiency loss and beam deviation caused by lens aberrations. Further power scaling is limited not only by enhanced SPM—which worsens spectral modulation—but also by the peak power tolerance of the PCF itself.

The single-transmission-grating compressor provides a compact structure and facilitates system integration. The distance between grating pairs and the grating's diffraction angle are critical factors governing the dispersion provided by the grating. The grating pair distance is directly proportional to the magnitude of the introduced GDD and TOD, while altering the diffraction angle simultaneously changes both the magnitude and the ratio of GDD to TOD. This system employs 1035 nm as the central wavelength, 1030 nm as the short wavelength, and 1040 nm as the long wavelength. The laser spectral width is set to 10 nm, with dispersion compensation achieved by adjusting the grating-mirror spacing. The laser beam is incident at a Littrow angle of 61.6°. The propagation paths for both the long and short wavelengths within the compressed grating are calculated separately, ensuring that the stretched spot is entirely reflected back by the mirror and received by the single transmission grating.

$$\Phi = 2 \cdot \frac{2\pi}{\lambda} \cdot \frac{L_g}{cos\theta}[1 + cos(\gamma - \theta)] - 2 \cdot \frac{2\pi}{d} \cdot L_g tan\theta \quad (2)$$

According to Equation (2), a conventional dual-grating compressor with a center wavelength of 1035 nm requires a propagation length of 30 cm to achieve GDD = -31.686×10^6 fs^2 and TOD = 409.965×10^6 fs^3, corresponding to D_2 = 55.75 ps/nm and D_3 = 1.1614 ps/nm^2. The overall spectral dispersion curve is shown in Figure 5a. The total propagation distance for the single transmission grating configuration is 63.1 cm. Based on an optical design centered at 1035 nm, the distance from the grating to the first 45° mirror is 33.12 cm, the spacing between the two 45° mirrors is 3.7 cm, and the distance from the second 45° mirror to the grating is 26.28 cm. Special attention was paid during the design process to avoid beam truncation caused by the two 45° mirrors. Through carefully adjusting the vertical distance of the compression gratings, the duration of the amplified pulse could be compressed to 245 fs, assuming a Gaussian pulse envelope at the maximum output power, as shown in Figure 5c. By carefully adjusting the vertical spacing of the compression grating, the duration of the amplified pulse can be compressed to 245 fs, assuming a Gaussian pulse envelope at maximum output power, as shown in Figure 5c. However, uncompensated higher-order dispersion caused by nonlinear effects results in a pulse pedestal in the corresponding autocorrelation trace, indicating a significant degradation in pulse quality. This was partly addressed by finely tuning the dispersion provided by the TCFBG. When the pulse duration is reduced to 207 fs, the pulse pedestal disappears from the autocorrelation trace, as shown in Figure 5d. At a central wavelength of 1035 nm, the laser exhibited a FWHM spectral bandwidth of 9.5 nm, corresponding to a Fourier-transform-limited pulse duration of 166 fs, indicating residual effects from higher-order dispersion and nonlinear phase.

Figure 5b shows the beam quality measured with a commercial M^2 meter (Spiricon M^2-200s). The M^2 of output 32 μJ pulse at a rep-rate of 1 MHz was quantified to be 1.04 and 1.05 for horizontal and vertical directions, respectively. The inset shows the well-confined Gaussian beam profile measured by a CCD camera at the average power of 32 W. These indicate that the fiber laser exhibited a high laser performance.

Monitoring was conducted for eight hours under stable operating conditions. As shown in Figure 6a, the root mean square (RMS) power fluctuation was only 0.25% at an output power of 32 W. A total of 33 sets of data were obtained by collecting spectral data every 15 min. The spectral stability plot (Figure 6b) exhibits a uniform banded structure with no observable fluctuations or diffusion phenomena. The system maintains all-fiber

transmission throughout laser generation and amplification, ensuring high stability and providing excellent resistance to temperature variations and mechanical vibrations. These characteristics establish a solid foundation for long-term reliable operation in industrial, medical, and defense applications.

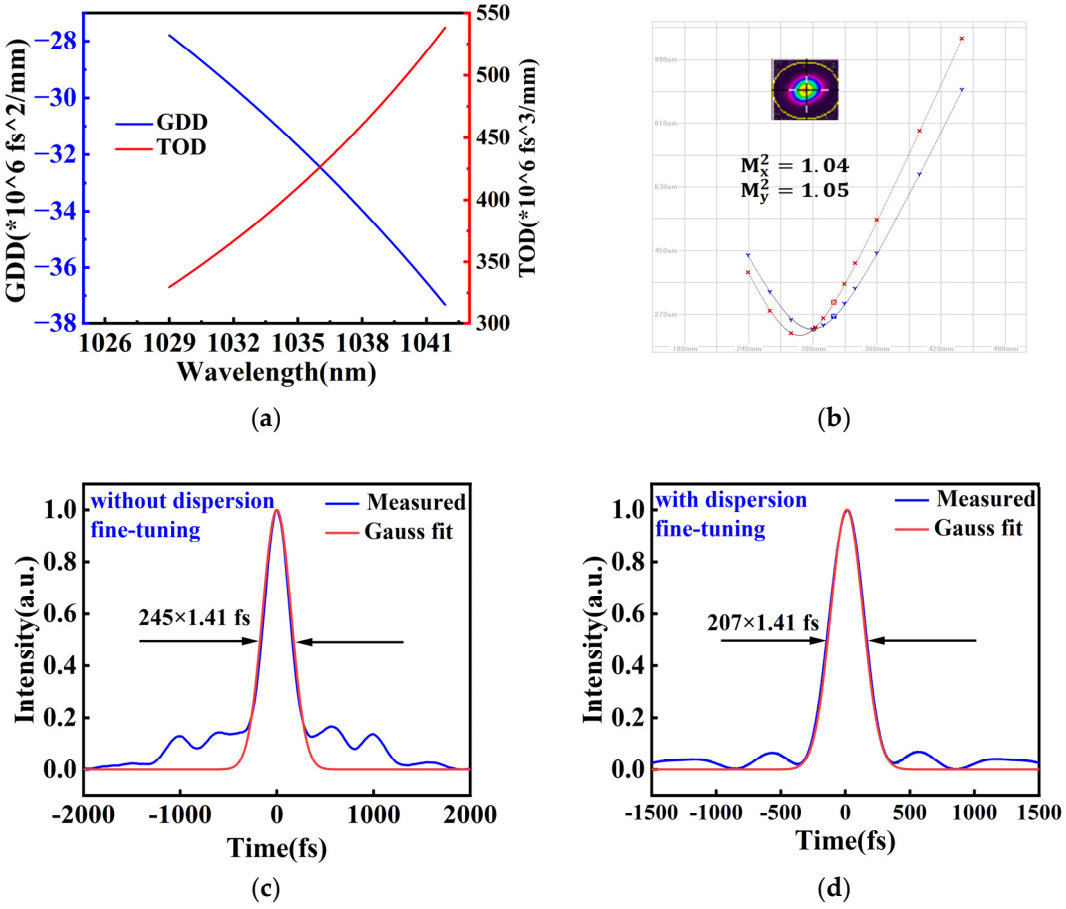


Figure 5. (**a**) Dispersion characteristics. (**b**) M^2 factor at the output power of 32 W. (**c**) Autocorrelation curve without TCBG dispersion adjustment at the highest output power. (**d**) Autocorrelation curve for adjusting TCBG dispersion at the highest output power.

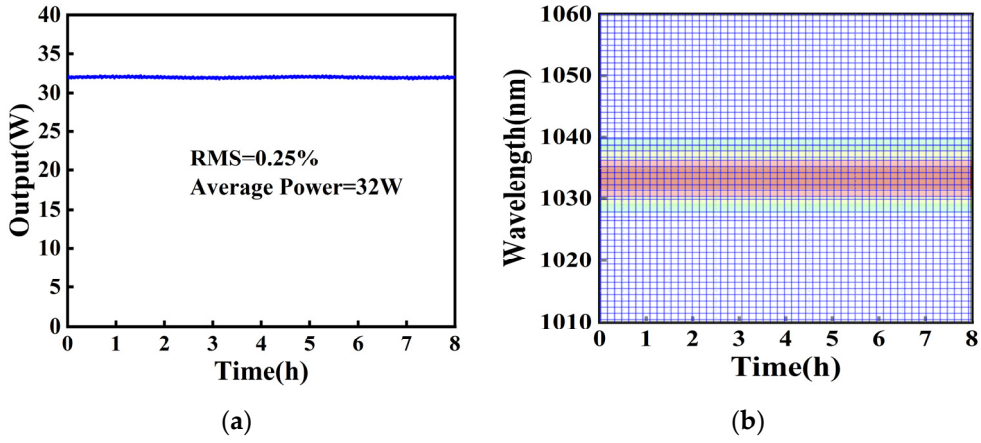


Figure 6. (**a**) Average power stability over eight hour; (**b**) Eight-hour spectral stability.

4. Conclusions

In summary, we have demonstrated a compact, high-power femtosecond fiber CPA system. By leveraging an all-PM-fiber front end, a short LMA gain fiber, and a matched TCFBG-grating dispersion scheme, it generates 32 μJ, 207 fs with 154.6 MW of peak

power at a 1 MHz repetition rate. The system achieves near-diffraction-limited output (M_x^2 = 1.04, M_y^2 = 1.05). It is anticipated that further advancements in next-generation gain fibers and spectral pre-shaping technologies [30] will enable increased power and reduced pulse duration. The laser system demonstrates unique advantages in metal processing and multiphoton imaging, owing to its high average power, high pulse energy, and excellent beam quality at a 1 MHz repetition rate [31,32].

Author Contributions: Conceptualization, X.S. and X.M.; methodology, X.S.; software, X.M.; validation, X.S., T.J. and Z.G.; formal analysis, J.Y.; investigation, X.Z.; resources, X.M.; data curation, X.S.; writing—original draft preparation, X.S.; writing—review and editing, G.Y.; visualization, Y.B.; supervision, J.C.; project administration, X.M.; funding acquisition, P.L. All authors have read and agreed to the published version of the manuscript.

Funding: This work was financially supported by the National Natural Science Foundation of China (62575007, 61905287); National Key Scientific Instrument and Equipment Development Projects of China (2022YFB3606203); Beijing Postdoctoral Science Foundation (2022ZZ-073); and Beijing Chaoyang District Postdoctoral Foundation.

Institutional Review Board Statement: Not applicable.

Informed Consent Statement: Not applicable.

Data Availability Statement: Data underlying the results presented in this paper are not publicly available at this time but may be obtained from the authors upon reasonable request.

Conflicts of Interest: The authors declare no conflicts of interest.

References

1. Li, J.; Zheng, Z.; Sheng, C.; Xia, Q. Endoscopic ureteral dilation balloon catheter for a difficult ureter: A new novel approach. *Urol. Int.* **2021**, *106*, 1246–1251. [CrossRef] [PubMed]
2. Weng, R.; Zhang, M.; Fan, G.; Jiao, W.; Lin, P.; Zhang, Z.; Zeng, D.; Yu, X. Research on a CDMA-based integrated single-terminal detection system for laser communication networking with micrometer-level disturbance error. *Opt. Commun.* **2025**, *586*, 131928. [CrossRef]
3. Lee, K.F.; Ding, X.; Hammond, T.; Fermann, M.E.; Vampa, G.; Corkum, P.B. Harmonic Generation in Solids with Direct Fiber Laser Pumping. *Opt. Lett.* **2017**, *42*, 1113. [CrossRef] [PubMed]
4. Kwon, D. Excess Intensity Noise in a Nonlinear Amplifying Loop-Mirror-Based Mode-Locked Laser from a Non-Reciprocal Phase Bias. *Photonics* **2024**, *11*, 1186. [CrossRef]
5. Liu, X.; Pang, M. Revealing the Buildup Dynamics of Harmonic Mode-Locking States in Ultrafast Lasers. *Laser Photonics Rev.* **2019**, *13*, 1800333. [CrossRef]
6. Xia, K.; Ren, N.; Lin, Q.; Li, T.; Gao, F.; Yang, H.; Song, S. Experimental Investigation of Femtosecond Laser Through-Hole Drilling of Stainless Steel with and without Transverse Magnetic Assistance. *Appl. Opt.* **2021**, *60*, 1399. [CrossRef]
7. Wang, C.; Zhang, S.; Luo, Z.; Ding, K.; Liu, B.; Duan, J. High-Quality Welding of Glass by a Femtosecond Laser Assisted with Silver Nanofilm. *Appl. Opt.* **2021**, *60*, 5360. [CrossRef]
8. Tan, Y.; Chu, W.; Wang, P.; Li, W.; Wang, Z.; Cheng, Y. Water-Assisted Laser Drilling of High-Aspect-Ratio 3D Microchannels in Glass with Spatiotemporally Focused Femtosecond Laser Pulses. *Opt. Mater. Express* **2019**, *9*, 1971–1978. [CrossRef]
9. Yoshitomi, D.; Takada, H.; Torizuka, K.; Kobayashi, Y. 100-W Average-Power Femtosecond Fiber Laser System with Variable Parameters for Rapid Optimization of Laser Processing. In Proceedings of the Conference on Lasers and Electro-Optics OSA, San Jose, CA, USA, 5–10 May 2019; pp. 1–2.
10. Yang, P.; Hao, T.; Hu, Z.; Fang, S.; Wang, J.; Zhu, J.; Wei, Z. Highly Stable Yb-Fiber Laser Amplifier of Delivering 32-μJ, 153-Fs Pulses at 1-MHz Repetition Rate. *Appl. Phys. B* **2018**, *124*, 169. [CrossRef]
11. Li, H.; Bu, X.; Shi, Y.; Peng, Z.; Xu, Y.; Cheng, Z.; Wang, P. High-power chirped pulse amplification based on Yb-doped rod-type PCF and nonlinear amplifying loop mirror oscillator. In Proceedings of the SPIE 2019 International Conference on Optical Instruments and Technology: Advanced Laser Technology and Applications, Beijing, China, 12 March 2020; p. 114370Q.
12. Huang, H.; Zhang, Y.; Teng, H.; Fang, S.; Wang, J.; Zhu, J.; Kaertner, F.; Chang, G.; Wei, Z. Pre-Chirp Managed Amplification of Circularly Polarized Pulses Using Chirped Mirrors for Pulse Compression. In Proceedings of the Conference on Lasers and Electro-Optics, San Jose, CA, USA, 5–10 May 2019; pp. 1–2.

13. Zhao, Q.; Gao, G.; Cong, Z.; Zhang, Z.; Liu, G.; Liu, Z.; Zhang, X.; Zhao, Z. High-Repetition-Rate, 50-μJ-Level, 1064-Nm, CPA Laser System Based on a Single-Stage Double-Pass Yb-Doped Rod-Type Fiber Amplifier. *Opt. Express* **2022**, *30*, 3611. [CrossRef]
14. Stutzki, F.; Jansen, F.; Eidam, T.; Jauregui, C.; Limpert, J.; Tünnermann, A. Robust single-mode high average power very large mode area fiber amplifiers. In Proceedings of the Advances in Optical Materials, Washington, DC, USA, 13–17 November 2011; p. AMB11.
15. Pedersen, M.E.V.; Johansen, M.M.; Olesen, A.S.; Michieletto, M.; Gaponenko, M.; Maack, M.D. 175 W Average Power from a Single-Core Rod Fiber-Based Chirped-Pulse-Amplification System. *Opt. Lett.* **2022**, *47*, 517. [CrossRef]
16. Li, F.; Yang, Z.; Zhao, W.; Li, Q.; Zhang, X.; Yang, X.; Zhang, W.; Wang, Y. 50 μJ Femtosecond Laser System Based on Strictly All-Fiber CPA Structure. *IEEE Photonics J.* **2016**, *8*, 1–6. [CrossRef]
17. Sun, R.; Jin, D.; Tan, F.; Wei, S.; Hong, C.; Xu, J.; Liu, J.; Wang, P. High-Power All-Fiber Femtosecond Chirped Pulse Amplification Based on Dispersive Wave and Chirped-Volume Bragg Grating. *Opt. Express* **2016**, *24*, 22806. [CrossRef] [PubMed]
18. Deng, D.; Zhang, H.; Gong, Q.; He, L.; Zu, J. 112-μJ 180-Fs Pulses at 1-kHz Repetition Rate from Yb-Doped Laser Based on Strictly All-Fiber CPA Structure. *IEEE Photonics J.* **2019**, *11*, 1–7. [CrossRef]
19. Tian, Z.; Qiu, H.; Wang, H.; Qian, K.; Luo, J.; Lin, S.; Du, J.; Chen, D.; Wang, Z.; Chen, Z.; et al. A Wide Spectrum Yb-Doped All-Fiber-Integrated Chirped Pulse Amplification System Based on Parabolic Shaping. *J. Nanoelectron. Optoelectron.* **2023**, *18*, 705–710. [CrossRef]
20. Tian, H.; Zhu, Z.; Lin, W.; Li, Z.; Wen, J.; Xiu, H.; Fan, Y.; Wei, C.; Wei, X.; Yang, Z. Stable Ultraviolet Ultrafast Laser Based on All-Polarization-Maintaining Fiber Femtosecond Laser. *Chin. Opt. Lett.* **2024**, *22*, 031404. [CrossRef]
21. Xiao, X.; Shi, W.; Gao, C.; Gui, Y.; Pang, M.; Zhou, G.; Leng, Y. Repetition-Rate Tunable Ultrafast Microjoule Yb-Fiber Lasers. *Chin. Opt. Lett.* **2025**, *23*, 071402. [CrossRef]
22. Lv, Z.; Yang, Z.; Li, F.; Yang, X.; Li, Q.; Zhang, X.; Wang, Y.; Zhao, W. High Power All-Polarization-Maintaining Photonic Crystal Fiber Monolithic Femtosecond Nonlinear Chirped-Pulse Amplifier. *Opt. Laser Technol.* **2018**, *100*, 282–285. [CrossRef]
23. Chang, H.; Cheng, Z.; Sun, R.; Peng, Z.; Yu, M.; You, Y.; Wang, M.; Wang, P. 172-fs, 27-μJ, Yb-Doped All-Fiber-Integrated Chirped Pulse Amplification System Based on Parabolic Evolution by Passive Spectral Amplitude Shaping. *Opt. Express* **2019**, *27*, 34103. [CrossRef]
24. Lü, R.; Teng, H.; Zhu, J.; Yu, Y.; Liu, W.; Chang, G.; Wei, Z. High Power Yb-Fiber Laser Amplifier Based on Nonlinear Chirped-Pulse Amplification at a Repetition Rate of 1 MHz. *Chin. Opt. Lett.* **2021**, *19*, 091401. [CrossRef]
25. Perry, M.D.; Ditmire, T.; Stuart, B.C. Self-Phase Modulation in Chirped-Pulse Amplification. *Opt. Lett.* **1994**, *19*, 2149–2151. [CrossRef]
26. Eidam, T.; Rothhardt, J.; Stutzki, F.; Jansen, F.; Hädrich, S.; Carstens, H.; Jauregui, C.; Limpert, J.; Tünnermann, A. Fiber Chirped-Pulse Amplification System Emitting 38 GW Peak Power. *Opt. Express* **2011**, *19*, 255. [CrossRef]
27. Liu, Y.; Krogen, P.; Schimpf, D.N.; Chang, G.; Keathley, P.; Kärtner, F.X. Compact, 200 MW Peak Power, 1 Mm Source with All-Fiber Front-End. In Proceedings of the CLEO Pacific Rim Conference, OSA, Hong Kong, China, 29 July–3 August 2018; pp. 1–2.
28. Ter-Mikirtychev, V. High-power fiber lasers. In *Fundals of Fiber Lasers and Fiber Amplifiers*; Springer International Publishing: Cham, Switzerland, 2014; pp. 213–244.
29. Agrawal, G.P. Chapter 4.2.—On the combined effects of SPM and normal dispersion leading to pulse shaping and spectral modulation. In *Nonlinear Fiber Optics*, 7th ed.; Academic Press: New York, NY, USA, 2019; pp. 136–141.
30. Gu, C.; Chang, Y.; Zhang, D.; Cheng, J.; Chen, S.-C. Femtosecond Laser Pulse Shaping at Megahertz Rate via a Digital Micromirror Device. *Opt. Lett.* **2015**, *40*, 4018. [CrossRef]
31. Shin, S.; Kim, J. Modeling Highly Efficient Femtosecond Laser Ablation of Aluminum for Cutting. *Sci Rep.* **2025**, *15*, 5418. [CrossRef]
32. Eisenberg, Y.; Wang, W.; Zhao, S.; Hebert, E.S.; Chen, Y.-H.; Ouzounov, D.G.; Takahashi, H.; Gruzdeva, A.; LaViolette, A.K.; Labaz, M.; et al. Efficient, Broadly Tunable, Hollow-Fiber Source of Megawatt Pulses for Multiphoton Microscopy. *Biomed. Opt. Express* **2025**, *16*, 415–425. [CrossRef]

Disclaimer/Publisher's Note: The statements, opinions and data contained in all publications are solely those of the individual author(s) and contributor(s) and not of MDPI and/or the editor(s). MDPI and/or the editor(s) disclaim responsibility for any injury to people or property resulting from any ideas, methods, instructions or products referred to in the content.